REPORT DOCUMENTATION PAGE

Form Approved
OMB No. 0704-0188

1. AGENCY USE ONLY (Leave blank)	2. REPORT DATE: 25 August 92	3. REPORT TYPE AND DATES COVERED: Reprint

4. TITLE AND SUBTITLE
Automatic Tornado Prediction with an Improved Mesocyclone-Detection Algorithm

5. FUNDING NUMBERS
PE 63707F
PR 2781
TA 01
WU 06

6. AUTHOR(S)
Paul R. Desrochers, Ralph J. Donaldson, Jr.*

7. PERFORMING ORGANIZATION NAME(S) AND ADDRESS(ES)
Phillips Lab/GPAP
Hanscom AFB
Massachusetts 01731-5000

8. PERFORMING ORGANIZATION REPORT NUMBER
PL-TR-92-2219

9. SPONSORING/MONITORING AGENCY NAME(S) AND ADDRESS(ES)

10. SPONSORING/MONITORING AGENCY REPORT NUMBER

11. SUPPLEMENTARY NOTES *Hughes STX Corporation, Lexington, Massachusetts
Reprinted from WEATHER AND FORECASTING, Vol. 7, No. 2, June 1992

12a. DISTRIBUTION/AVAILABILITY STATEMENT
Approved for public release; Distribution unlimited

12b. DISTRIBUTION CODE

13. ABSTRACT (Maximum 200 words)

A new and improved algorithm for automatic mesocyclone detection is presented and tested on 23 mesocyclonic storms. A small false-alarm rate (4%) and high probability of detection (83%) are achieved for mesocyclone classification. A unique innovation of the algorithm is the automatic assessment of mesocyclone tornado potential. This is accomplished using excess rotational kinetic energy (ERKE), a form of rotational kinetic energy that is tailored for mesocyclonic shear. ERKE provides a measure of low- to midtropospheric mesocyclone intensification that is indicative of impending tornado formation. The quantitative determination provided by ERKE is a much better indicator of storm severity than is simple mesocyclone identification. Median lead times of over 30 min are provided for our small sample by ERKE for strong and violent tornadoes with a false-alarm rate of less than 5%.

14. SUBJECT TERMS: Tornado forecasting, Mesocyclones	15. NUMBER OF PAGES: 16
	16. PRICE CODE

17. SECURITY CLASSIFICATION OF REPORT	18. SECURITY CLASSIFICATION OF THIS PAGE	19. SECURITY CLASSIFICATION OF ABSTRACT	20. LIMITATION OF ABSTRACT
Unclassified	Unclassified	Unclassified	SAR

Reprinted from WEATHER AND FORECASTING, Vol. 7, No. 2, June 1992
American Meteorological Society

Automatic Tornado Prediction with an Improved Mesocyclone-Detection Algorithm

PAUL R. DESROCHERS

Phillips Laboratory, Geophysics Directorate, Hanscom AFB, Massachusetts

RALPH J. DONALDSON, JR.

Hughes STX Corporation, Lexington, Massachusetts

(Manuscript received 14 June 1991, in final form 2 January 1992)

ABSTRACT

A new and improved algorithm for automatic mesocyclone detection is presented and tested on 23 mesocyclonic storms. A small false-alarm rate (4%) and high probability of detection (83%) are achieved for mesocyclone classification. A unique innovation of the algorithm is the automatic assessment of mesocyclone tornado potential. This is accomplished using excess rotational kinetic energy (ERKE), a form of rotational kinetic energy that is tailored for mesocyclonic shear. ERKE provides a measure of low- to midtropospheric mesocyclone intensification that is indicative of impending tornado formation. The quantitative determination provided by ERKE is a much better indicator of storm severity than is simple mesocyclone identification. Median lead times of over 30 min are provided for our small sample by ERKE for strong and violent tornadoes with a false-alarm rate of less than 5%.

1. Introduction

Mesocyclones are organized rotations in severe thunderstorms, averaging 5.7 km in diameter, that, when fully developed, can extend from near the ground to the upper troposphere (Burgess et al. 1982). Mesocyclones were first detected with Doppler radar by Donaldson et al. (1969) in Massachusetts. Many more were subsequently detected by Burgess (1976) in Oklahoma. Burgess found that their identification in a storm is a good indication that severe weather will follow, because over 90% of the mesocyclones he detected were associated with some type of severe weather event such as large hail, strong winds, or tornadoes.

Mesocyclones can be readily detected by single-Doppler radar. This has brought much hope for and interest in Next Generation Weather Radar (NEXRAD), the soon-to-be-deployed-nationwide S-band (10-cm wavelength) Doppler radar system. NEXRAD radars will offer automated analyses to improve forecasters' ability to provide timely warning of hazardous events. Included in the NEXRAD arsenal is a mesocyclone detection algorithm (Zrnić et al. 1985a). Desrochers (1991), building on this and other algorithms, has designed an improved mesocyclone-detection algorithm that achieves a quantitative classification of several measures of mesocyclone intensity.

Corresponding author address: Paul R. Desrochers, Phillips Laboratory, Geophysics Directorate, Hanscom AFB, Massachusetts, 01731-5000.

In addition to basic mesocyclone detection, the new algorithm offers improved discrimination of tornadic storms. In a recent survey, Burgess and Lemon (1990) found that somewhat greater than half of all mesocyclonic storms produce tornadoes. However, automated detection is revealing that nontornadic mesocyclones comprise the majority, although many are weak and short lived (Burgess and Lemon 1991). Those mesocyclones associated with tornadoes generally precede the earliest tornado by 20 min on average (JDOP Staff 1979). A technique developed recently by Donaldson and Desrochers (1990) permits tornadic mesocyclones to be identified with an extremely low false-alarm rate and with lead times almost as large as by mesocyclone detection alone. Automation of this technique is an integral function of the new algorithm.

In section 2 we survey mesocyclone development and the criteria used to detect rotation with single-Doppler radar. Early automated mesocyclone detection algorithms are presented in section 3. Section 4 addresses mesocyclone utilization for tornado prediction. A description of the present algorithm is provided in section 5. Test results from 23 mesocyclonic storms are given in section 6.

2. Mesocyclone development

The mesocyclone is a rotating column of air associated with the convective updraft and/or downdraft of a severe thunderstorm. Mesocyclones form under limited conditions of vertical wind shear and buoyancy where a long-lived updraft can be supported (Weisman

and Klemp 1982). Incipient rotation occurs at midtropospheric levels in association with the development of the updraft, through tilting of environmental vorticity (Rotunno 1981; Davies-Jones 1984).

Mesocyclone development to the mature stage is marked by expansion both upward and downward. Flow at low levels generally consists of a combination of convergence and rotation. At midlevels there is pure rotation, and this gives way to divergence and rotation at higher levels (Burgess et al. 1982). The mesocyclone is sometimes observed to be capped by pure divergence in the upper troposphere (Lemon and Burgess 1980). The most intense tornadoes are likely to occur when the mesocyclone intensifies at low levels (Lemon and Doswell 1979).

Mesocyclones often undergo a cyclic process where the initial primary updraft is undercut by the gust front, and a new updraft and mesocyclone forms to the right in a zone of preferable pressure forcing (Brandes 1978; Ray et al. 1981). Whereas the initial mesocyclone of a storm undergoes a lengthy evolutionary process (31 min to maturity, and 91-min lifetime) in conjunction with the developing flow field of a storm, subsequent mesocyclones develop very quickly (9 min) and are shorter lived (45 min) (Burgess et al. 1982). The rapid development of subsequent mesocyclones is apparently due to their growth in an already vorticity-rich environment established by antecedent mesocyclones (Johnson et al. 1987).

The mesocyclone is modeled by a Rankine combined vortex containing a core region where velocity increases linearly out to a ring of maximum velocity, and an outer region of potential flow where velocity decreases inversely proportional to distance (Fig. 1a). The maximum velocities of the core are observed by radar only at the two points where velocity is directed along the beam. When sampled by a horizontally scanning radar, the mesocyclone appears as a velocity couplet, as shown in Fig. 1b, if the mesocyclone core subtends an angle larger than the radar beam.

In practice the mesocyclone does not always resemble a Rankine vortex. The entire mesocyclone may contain one or more circulations (Burgess et al. 1982), and may become quite convoluted by the time of tornado formation (Zrnić et al. 1985b). Mesocyclone appearance will vary greatly with range from the radar, the degree of convergence or divergence contained in the circulation, and the extent of feature asymmetry (Brown and Wood 1991).

Not all velocity couplets are associated with rotation; they can represent nonrotational shear such as flow around an obstacle (Wood and Brown 1983). Consequently, Donaldson (1970) proposed criteria to establish the likelihood of rotation. These criteria comprise shear across the feature, vertical structure, and persistence. Burgess (1976) verified these through observations, and the criteria were tested operationally during the Joint Doppler Operational Program (JDOP)

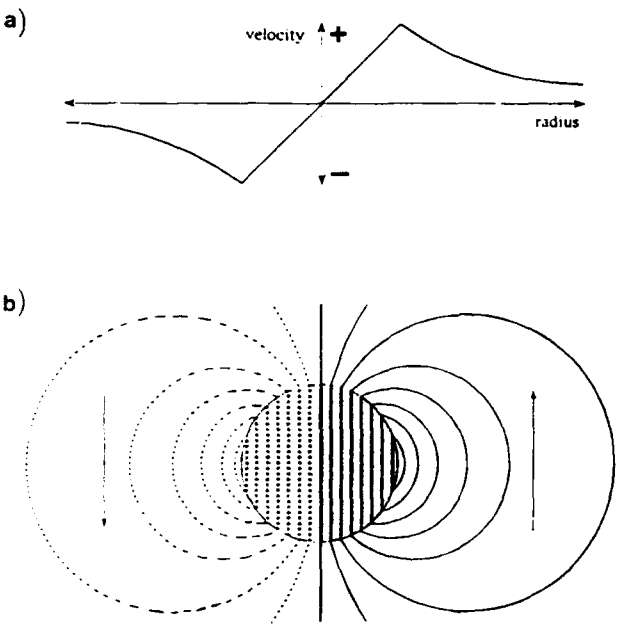

FIG. 1. Theoretical mesocyclone profile described by a Rankine combined vortex. (a) Velocity profile across the mesocyclone central axis. Positive (+) and negative (−) velocity signs indicate flow toward and away from the central axis. (b) Idealized view of mesocyclone by single-Doppler radar located in the direction toward the bottom of the page. Dashed contours represent flow toward the radar, and solid contours represent flow away. Zero Doppler velocity is represented by the thick, solid line. The mesocyclone core region is shaded. This figure illustrates the general appearance of the "velocity couplet," where velocity peaks of opposite sign are diametrically opposed.

(JDOP Staff 1979). The JDOP criteria for mesocyclone detection within 230 km of the radar are given below.

- Shear of 0.005 s^{-1} between closed isodops of opposite sign. The shear axis is generally oriented in the azimuthal direction but may deviate as much as 45° from this axis.
- The mesocyclone shear pattern extends vertically at least 3 km.
- The mesocyclone signature persists for a time equal to half its rotation period, estimated by the inverse of shear across the velocity couplet multiplied by π.

With the JDOP criteria, we can not identify rotation as early as it occurs in a storm, but these criteria do not appear to be excessively restrictive, as there is, in most cases, at least 20 min lead time between mesocyclone identification and appearance of the first tornado.

3. Early mesocyclone detection algorithms

Automated detection of the mesocyclone was made possible by the invention of pattern vectors by Hennington and Burgess (1981). Key to this is the detection of the azimuthal velocity couplet (Fig. 1b), which is

characteristic of rotation. The most conservative quantity for identifying the mesocyclone is the sign of the azimuthal velocity gradient, because it is relatively insensitive to inhomogeneities of the core. The locations where the velocity trend changes from one sign to the other at a constant range in the azimuthal direction define the end points that comprise a pattern vector. Since radars sample at discrete range intervals, a series of discrete pattern vectors exist through the mesocyclone (Fig. 2). The outline produced by pattern vectors that extend across the center line of the mesocyclone is known as the pattern vector envelope. This shape is characteristic of mesocyclones and is useful for mesocyclone identification.

The elegance of pattern vectors lies in their concise representation of the important elements of the mesocyclone core; only the beginning and ending points are needed to describe a pattern vector. These points represent the maximum relative incoming and outgoing velocities at a particular range through the mesocyclone. Through simple association criteria, pattern vectors can be combined into a shear feature to reveal the mesocyclone pattern vector envelope, which provides adequate information to determine the mesocyclone core radius and its maximum rotational velocity.

In summary, mesocyclone identification involves the detection of pattern vectors, the association of pattern vectors from the same elevation scan into two-dimensional (2D) shear features, and the association of 2D shear features from differing elevations into three-dimensional (3D) features to satisfy some structural criteria. Zrnić et al. (1985a) formulated these ideas into an algorithm and tested it on numerous cases. Wieler (1986) improved on the basic algorithm design by incorporating resolution adjustable thresholds for pattern vectors and by permitting, in addition, the detection of anticyclonically rotating mesocyclones (mesoanticyclones).

4. Predicting mesocyclone-associated tornadoes

Supercell storms produce the most intense and long-lived tornadoes, and, therefore, the most life-threatening tornadoes. One hope for Doppler radar is that it will greatly improve tornado warnings by permitting direct detection of the tornado vortex within these storms (Atlas 1963; Lhermitte 1964). Indeed, Brown et al. (1978) found that a tornadic vortex signature (TVS) can sometimes be detected aloft prior to tornado touchdown. The TVS is seen as a small velocity couplet ($\sim$1 km) with very large azimuthal shear ($\sim$0.05 s^{-1}). When a TVS is detected, tornado appearance usually accompanies or follows. One severe operational limitation of the TVS, however, is the effective range of detection. Pencil-beam radars (1° half-power beamwidth) permit TVS detection to only about 40 km for all but the largest and most powerful tornadoes. Even at ranges under 40 km, a small tornado may appear without a detectable TVS.

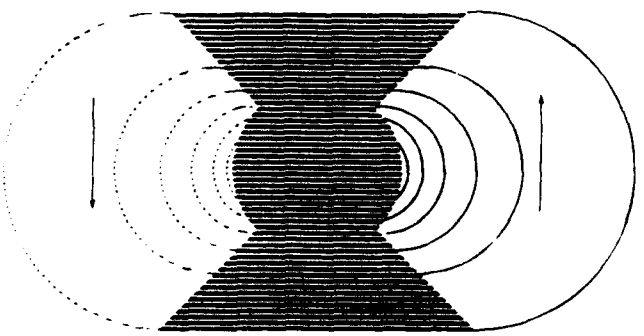

FIG. 2. An example of the pattern vectors (thick horizontal lines) and the pattern vector envelope that comprise the mesocyclone velocity couplet.

The mesocyclone, as a parent vortex for tornadoes, offers a considerable range advantage over the TVS for detection of tornado hazards. Although we do not yet fully understand the processes that lead to tornado formation, the mesocyclone is statistically tied to tornado occurrence; roughly 50% of mesocyclones cited by Burgess and Lemon (1990) were tornadic. With improved detection techniques, such as discussed herein and by Burgess and Lemon (1991), it is becoming apparent that a much smaller portion of mesocyclones are tornadic than once believed, perhaps less than 40%. Operational warnings would, therefore, benefit from a further delineation of storm type. Burgess (1976) initiated an effort to identify distinguishing characteristics of tornadic mesocyclones. He evaluated 37 mesocyclones to determine if variations in size, shear, or rotational velocity exist between those that are tornadic and those that are not. He found none, except for those that produced violent tornadoes. These tend to be taller, more narrow, and have greater shear. These results are supported by Burgess and Lemon (1990), where a larger dataset was examined.

Donaldson and Desrochers (1985) examined mesocyclone rotational kinetic energy (RKE) as a possible identifier of tornadic mesocyclones. Since features that do not produce tornadoes, such as extratropical cyclones, can have greater RKE than mesocyclones, they tailored RKE for mesocyclones. They proposed a parameter called excess rotational kinetic energy (ERKE), given by

$$\mathrm{ERKE} = \rho\pi\Delta h r^2 (V - rS_m)^2/4, \qquad (1)$$

where ρ is the air density, Δh the vertical thickness, r the feature radius, V its maximum rotational velocity, and S_m is an arbitrary shear threshold nominally set at 0.005 s^{-1}. We assign ERKE to zero for $rS_m \geq V$. When $S_m = 0$, ERKE is identical to RKE. All the necessary values for determining ERKE, except ρ, can be obtained from the mesocyclone velocity couplet. Air density is obtained from a standard atmosphere July sounding for 30°N latitude (U.S. Standard Atmosphere Supplement 1966) to correspond to our Oklahoma

dataset. The precise air density is not felt to be important, but the standard density distribution does provide the desired benefit of a greater weighting of ERKE at low levels.

We further define 2D ERKE where Δh is set to 1 m. Three-dimensional ERKE is obtained by integrating 2D ERKE from differing elevations over some specified thickness.

Donaldson and Desrochers (1990) tested ERKE on 17 mesocyclonic storms that were analyzed by subjective analysis of the Doppler radial velocities. These consisted of two that produced violent tornadoes [F4 according to the Fujita (1981) intensity scale], five that produced strong tornadoes (F2 and F3), one that produced a weak tornado (F1), and nine that were not tornadic. Although the technique does not show much skill for predicting weak tornadoes, it is extremely effective for more intense ones. They found that 3D ERKE integrated over the lower troposphere was effective in discriminating between the storms producing strong tornadoes and lesser storms. They could discriminate these in all but one case of their small sample. In addition, a median lead time of almost 20 min was provided to the first strong tornado of a storm. Even better results were achieved for the two storms with violent tornadoes. These were easily distinguished from the other storms by ERKE magnitude. Lead times of 28 and 134 min were obtained, with no false alarms.

Initially, in tornadic storms, 2D ERKE is greatest at middle levels, 5 to 8 km. As the mesocyclone develops, ERKE intensifies at lower levels and often exceeds the values at middle levels prior to tornado formation. This is borne out well by the Del City, Oklahoma, storm of 20 May 1977, which produced two strong tornadoes (Fig. 3). Here we show the maximum 2D ERKE and the height at which it occurred. ERKE magnitude is normalized by the value associated with a typical mature mesocyclone, what we term a climatological mature mesocyclone (CMM) from statistics of size and rotational velocity compiled by Burgess et al. (1982). The 2D ERKE associated with a climatological mature mesocyclone ($S_m = 0.005\ s^{-1}$) has a value of $5.3 \times 10^8\ J\ m^{-1}$. We assign this the value 1 CMM. The mesocyclone height in the lower part of Fig. 3 is a weighted height, weighted with regard to 2D ERKE magnitude. Summing over all elevations for which the mesocyclone velocity couplet is observed,

$$\text{weighted height} = \frac{\sum (\text{height})(\text{2D ERKE})}{\sum (\text{2D ERKE})}. \quad (2)$$

In nontornadic storms, the mesocyclone does not appear to intensify at low levels, although the intensity at midlevels can be greater than the low-level intensification of some tornadic storms. Tornado formation does not seem related only to mesocyclone intensity, but specifically to low-level intensification (Burgess et al. 1982; Desrochers et al. 1986).

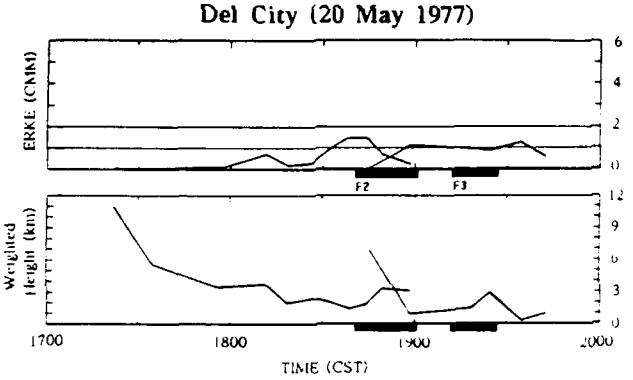

FIG. 3. Typical lifetime of a tornadic mesocyclone as depicted by ERKE. The top figure shows the maximum two-dimensional ERKE [Δh = 1 m in (1)] in a volume normalized in units of CMM. The bottom figure shows the height of ERKE, weighted with regard to ERKE magnitude. Tornado duration is indicated by the thick bars at the bottom of each figure. (Adapted from Desrochers et al. 1986.)

It is important to note that mesocyclones are not the only source of tornadoes. For example, tornadoes are occasionally observed to form along gust fronts (Wilson 1986). These varieties are generally weak and short lived. Tornadoes can also form early in the development stage of a storm, in association with rapidly developing cumuli (Burgess and Donaldson 1979). These too are generally weak (Bluestein 1985), but there are exceptions. Perturbational swirls that develop along surface convergence boundaries can be spun up to tornado intensity when they happen upon the updraft of rapidly growing cumuli (Wakimoto and Wilson 1989; Brady and Szoke 1989). It is estimated that tornadoes formed in this way can occasionally achieve intensity as great as F3 by simple stretching of the existing low-level vertical vorticity by a strong updraft (Wakimoto and Wilson 1989).

The question of why ERKE "works" for mesocyclonic storms is not one we have a complete answer to at present. Numerical simulations (Klemp and Rotunno 1983; Rotunno and Klemp 1985) and observations (Brandes 1981) suggest that low-level mesocyclone intensification provides a vorticity source for tornado development. ERKE provides a measure of this intensification that is responsive to increases in both rotational velocity and vorticity [for solid-body rotation, like the mesocyclone core, vertical vorticity is proportional to rotational shear (e.g., Holton 1979)]. The manner in which the vorticity becomes concentrated in tornadic scale (i.e., through stretching or diabatic processes) is still a matter of speculation.

5. The automated mesocyclone-detection and tornado-prediction algorithm

The mesocyclone algorithm presented here represents a further improvement in detection design. We have concentrated on improving the accuracy of feature

estimations such as mesocyclone size and rotational velocity, and utilizing algorithm analyses for tornado prediction. A welcome by-product is the improved detection of weak and small mesocyclones.

The steps for mesocyclone detection by the present algorithm are given in Fig. 4. This flow diagram is meant to provide the reader with a general idea of algorithm processes and structure. In this section we describe the primary innovations offered by the algorithm. Technical aspects of the algorithm are given in appendix A. A detailed description of the algorithm is available in Desrochers (1991).

a. Analysis capabilities and techniques

A technique for isolating the velocity maxima of the couplet was developed. The velocity couplet endpoint locations and velocity values are determined by a process that weights toward the largest velocity values. The technique provides accurate estimates of mesocyclone size and velocity, within 4% of values arrived at through subjective analysis of the Doppler fields. This is important because estimations of mesocyclone severity through ERKE depend on accurate estimations of feature size and rotational velocity.

Most mesocyclone scans display some combination of rotation and divergence, and the analysis technique permits this determination. Each component is a function of the velocity couplet orientation angle (θ) measured orthogonal to the radar beam. An example of θ, along with velocity couplet endpoint determinations produced by the technique, is shown in Fig. 5. Here, θ indicates a mesocyclone flow comprised of a combination of rotation and convergence. Rotational velocity is given by the average magnitude of the two endpoint Doppler velocities multiplied by cosine (θ). Mesocyclone diameter is defined as the distance between the velocity couplet end points.

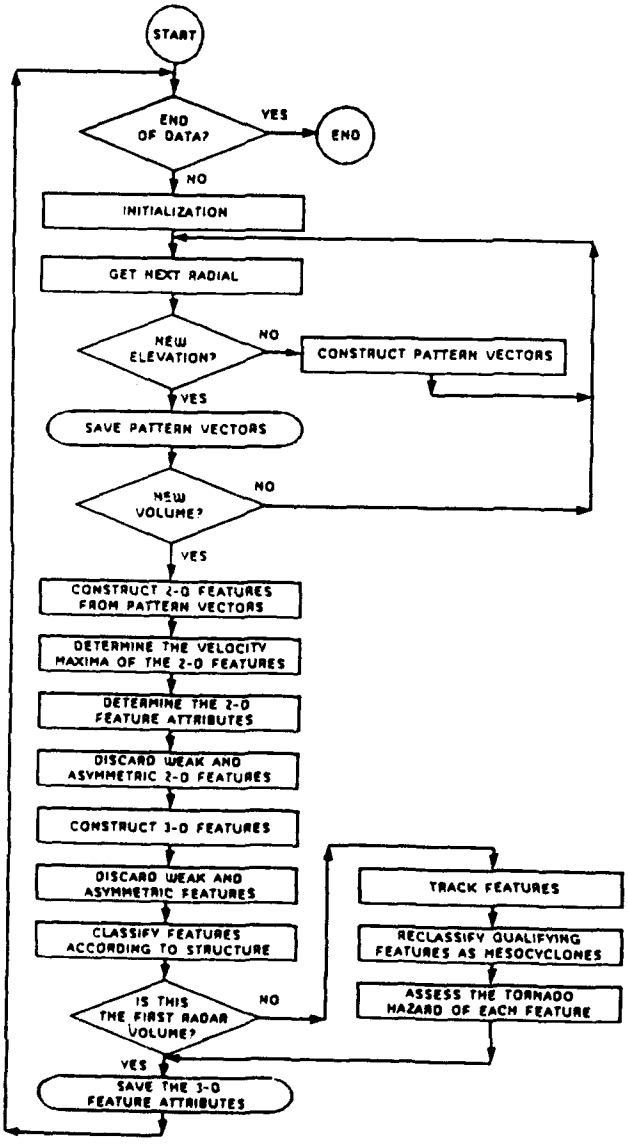

FIG. 4. Flow diagram of the general operations for the mesocyclone-detection and tornado-prediction algorithm.

b. Resolution corrections

The ability of radar to resolve a feature is a function of the beamwidth (typically 1° for a pencil-beam radar) and the size of the feature. Rotation can be detected when the beamwidth is less than the core radius. Rotation may be detected with poorer resolution if the feature placement is such that the velocity couplet maxima happen to be sampled by different beams.

Brown and Lemon (1976) developed a theoretical model of how a Rankine combined vortex would appear with varying resolution. Figure 6, adapted from their work, presents normalization factors for tangential velocity and vortex size for various radar beamwidth to vortex core-radius (BW/CR) ratios. As resolution decreases, a vortex will appear larger than actual size and of lesser intensity. Resolution correction can be applied only up to BW/CR = 1. At larger ratios the actual size of a vortex is ambiguous.

Pattern vector thresholds (10 m s^{-1} and 0.003 s^{-1}) and the application of the Brown and Lemon corrections permit weak mesocyclones of 3- and 5-km diameter to be detected and corrected to a range of 85 and 145 km, respectively, with a 1° beam. An average mature mesocyclone (diameter of 6 km and rotational shear of 0.008 s^{-1}) can be accurately detected and corrected to a range of 170 km with the present thresholds. The same mesocyclone may be detected to the 230-km operational range specified by the NEXRAD Joint System Program Office (1986), although only a partial correction can be made for resolution. Beyond this range, the earth's curvature becomes comparable to the radar resolution as a factor limiting mesocyclone detection. More significant mesocyclones have been detected to ranges beyond 300 km (JDOP Staff 1979), but the earth's curvature restricted our view of them to the middle and upper troposphere.

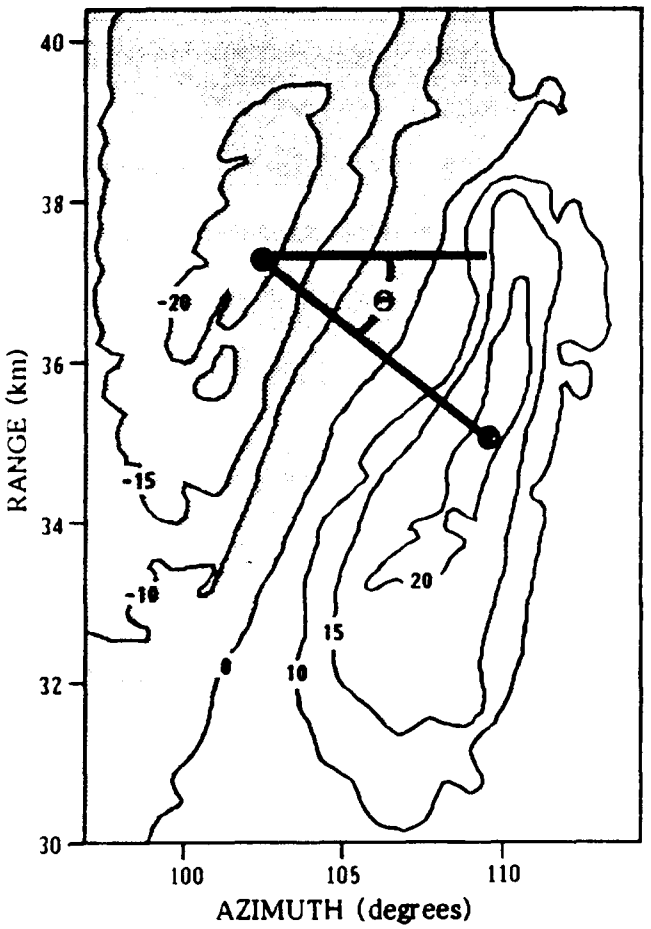

FIG. 5. An example of the velocity couplet analysis provided by the mesocyclone algorithm. Contours were determined from subjective analysis of the Doppler field and are labeled in meters per second. Flow toward (away from) the radar is shaded (nonshaded). Algorithm-determined velocity couplet end points are indicated by the large dots. These permit the mesocyclone orientation angle (θ) to be determined. This example shows a flow field having a combination of rotation and convergence. Data are from the Del City, Oklahoma, mesocyclone (20 May 1977) at 0.8° and 1832 CST.

c. *Feature classification*

Mesocyclone classification by the algorithm uses as a basis the JDOP criteria (JDOP Staff 1979). These criteria have been refined somewhat and additional requirements for feature structure have been added. There are six basic stages of feature classification, including three stages of mesocyclone classification. These are: *shear feature, 2D couplet, 3D couplet, provisional mesocyclone, mesocyclone,* and *TVS*. Anticyclonic features may also be identified, although this aspect of the algorithm has not been utilized.

Mesocyclone classification is a graduated process that begins with *shear feature,* as discussed in section 3. A shape criterion, satisfied when the maximum azimuthal and radial dimensions of the pattern vector envelope are within a factor of 2 of each other, determines classification upgrade to *couplet.* Couplets are separated into two categories, 2D or 3D, depending on whether the feature is based on data from one or more than one elevation. For 3D couplets, shape is the average shape of all the elevations.

A 3D couplet may be upgraded to one of three categories of mesocyclone. Three-dimensional features with at least two adjacent elevations displaying mesocyclonic shear of 0.005 s^{-1} and with an inclusive height interval of at least 3 km of mesocyclonic shear are reclassified as a *provisional mesocyclone.* Included in the thickness of mesocyclonic shear is the thickness associated with the half-power beamwidth, 1° for this data, in order to normalize the detection criteria with range. A further upgrade to *mesocyclone* is accomplished by detecting the same provisional mesocyclonic feature during the following volume scan.

In addition to basic mesocyclone detection, the algorithm can identify shear of tornadic strength when it exists within a mesocyclone. A mesocyclone is graduated to a *TVS* when excessive shear is identified over two consecutive elevations. The shear threshold used to define a TVS is the same as used in JDOP, 0.05 s^{-1} (JDOP Staff 1979). TVS shear on consecutive elevations must be within 1 km horizontally. Also, TVS shear at a particular elevation is identified when TVS shear extends over at least three adjacent pattern vec-

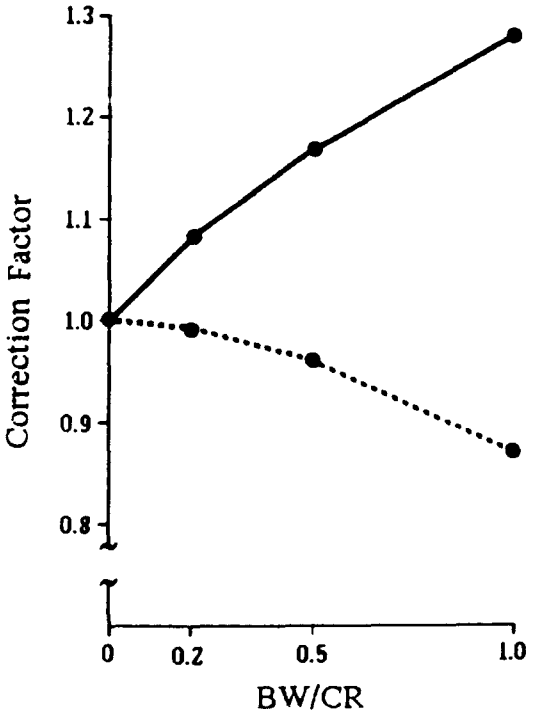

FIG. 6. Resolution correction factors for velocity (solid lines) and azimuthal diameter (dotted lines) as a function of the radar beamwidth to mesocyclone core-radius (BW/CR) ratio. (Adapted from Brown and Lemon 1976.)

tors. This implies a minimum radial extent and, therefore, only large tornadoes will be identified. TVS detection is considered secondary to tornado prediction by mesocyclone ERKE because TVS detection is more severely restricted by range. In fact, mesocyclone ERKE often permits the prediction of tornadoes at ranges many times farther than the maximum range at which a TVS could be resolved by radar. Also, the TVS, when it is observed, most frequently provides considerably less warning time than the mesocyclone.

d. Determination of tornado predictors

The algorithm generates 3D values of ERKE for use in tornado warning, as well as 3D values of velocity and shear. Three-dimensional quantifications of the mesocyclone are preferable to 2D ones, since they reduce the impact of the erroneous analysis of a single elevation.

Three-dimensional values are obtained by integrating over the 2D values of a 3D feature from the surface (zero km) to some specified height. The 2D values are set to zero at the surface and at levels of a 3D feature where a 2D feature was not found. It is assumed that 2D values vary linearly between observation levels. Integration heights of 0–4 km to 0–7 km in 1-km intervals are generated. For ERKE, shear thresholds in (1) of 0.005, 0.006, and 0.007 s^{-1} are examined. The range of integration heights and shear thresholds facilitates algorithm tuning.

e. Feature tracking and tornado prediction

A tracking routine monitors features from one volume scan to the next. This is necessary to satisfy the persistence criteria of the JDOP rules for mesocyclone classification, and for tornado likelihood estimations.

Finally, the algorithm determines the tornadic threat associated with each feature. A tornado hazard becomes more likely as ERKE is observed to increase in a storm. Details of the lead times provided and the discrimination capability are discussed in the following section.

6. Test cases and results

We have tested the algorithm on data from five days in Oklahoma. These contain 23 mesocyclonic storms, verified by subjective Doppler interpretations, ranging in intensity from marginal to violently tornadic. Two of these storms produced violent tornadoes (F4) and five others produced strong tornadoes (F2–F3), but none are believed to have produced only weak (F0–F1) tornadoes. The remaining 16 of the mesocyclonic storms were nontornadic. A list of the cases is shown in Table 1. The algorithm identified 20 mesocyclonic storms using standard JDOP criteria. These include four that we have labeled "transient mesocyclone" because they achieved the mesocyclone designation for only one volume scan. Some of the mesocyclones were examined in our earlier manual study (Donaldson and Desrochers 1990). The data also contain some additional mesocyclones, revealed by the algorithm, that did not originally attract our attention because they were weak and/or short lived. Besides mesocyclones, numerous less-significant features (shear features, couplets, and provisional mesocyclones) were identified by the algorithm. The anticyclonic detection capability of the algorithm has not been utilized for this study.

Analysis times cover the lifetimes of all mesocyclones except Vanoss (29 April 1978) and Clinton (22 May 1981). Our coverage of these was sufficient to verify the mesocyclones, and to distinguish by ERKE that Clinton was tornadic while Vanoss was not. Vanoss was at all times extremely weak, but we do not know if Clinton intensified further at a later time to produce a false alarm for violent tornadoes by ERKE. Volume scan duration in all storms ranged from 3 to 20 min, with a mean duration of 6 min.

Tornado touchdown times and intensities were available from the National Severe Storms Laboratory (Don Burgess, personal communication) and from *Storm Data* (NOAA 1977, 1978, 1981). Damage surveys were available for all storms except for Arapaho, which produced three reported tornadoes. Intensities for Arapaho are estimated from the limited available damage descriptions. Many tornado times were given to the nearest minute, some to the nearest 5 min, and only Arapaho to the nearest 15 min.

a. Mesocyclone detection

All features identified as mesocyclones by the algorithm were verified through subjective analysis of the Doppler velocity field of the data. The same preprocessing techniques (see appendix B) were applied to the algorithmic and manual data to ensure an identical base for comparison. In most cases, every elevation scan of a mesocyclone was examined subjectively. Exceptions were Binger and Del City, where some of the volume scans contain over 20 elevations. In these, at least every other elevation was examined. In some of the storms, the maximum height of the mesocyclone could not always be verified because of scanning limitations and severe velocity aliasing. Our coverage always included 0 to 7 km above ground level (AGL).

To help assure that all marginal mesocyclones were identified, the data were reprocessed with the shear threshold [S_m in (1)] for mesocyclone identification reduced to 90% of the JDOP value. Any additional mesocyclones identified with the reduced threshold were also verified by visual inspection. Therefore, the data consist of 26 algorithm-identified mesocyclonic storms that were verified by visual inspection. Table 1 lists all these cases and their classification as given by the regular JDOP shear threshold of 0.005 s^{-1}.

TABLE 1. Significant features of the dataset.

a) Algorithm-identified mesocyclonic storms using full JDOP thresholds.

Date	Storm name	Classification		Tornadoes	Feature duration (min)	Mesocyclone range (km)	Maximum ERKE (CMM)
		Algorithm	Manual	W S V			
5/22/81	Binger	meso	meso	3 1 1	277	44–165	3.09
4/30/78	Piedmont	meso	meso	3 1 1	173	49–76	3.07
5/22/81	?Arapaho	meso	meso	1? 2? 0?	124	141–174	2.90
5/22/81	Cordell	meso	meso	0 1 0	174	118–164	1.41
5/20/77	Fort Cobb	meso	meso	0 2 0	80	50–71	1.36
5/22/81	*Clinton	meso	meso	0 1 0	35	144–157	0.86
5/20/77	Del City	meso	meso	0 2 0	73	37–71	0.68
4/30/78	El Reno	meso	meso	0 0 0	108	44–63	0.49
4/29/78	Ada	meso	meso	0 0 0	136	68–101	0.41
4/30/78	Rush Springs	meso	meso	0 0 0	79	64–69	0.37
4/29/78	Slick	T-meso	P-meso	0 0 0	37	125	0.25
4/29/78	Sylvian	meso	meso	0 0 0	52	78–94	0.23
4/29/78	Konawa	meso	meso	0 0 0	99	64–79	0.17
4/29/78	Wynnewood	meso	meso	0 0 0	42	77–78	0.05
5/22/81	Waynoka	meso	meso	0 0 0	100	199–200	0.02
5/20/77	Sterling	meso	T-meso	0 0 0	35	58–94	0.02
4/29/78	*Vanoss	meso	meso	0 0 0	58	79–81	0.01
5/22/81	Blain	T-meso	meso	0 0 0	56	110	0.02
4/30/78	Cashion	T-meso	T-meso	0 0 0	57	62	0.00
5/22/81	Butler	T-meso	T-meso	0 0 0	54	157	0.00
b) Additional mesocyclonic storms identified with reduced JDOP shear threshold.							
4/09/78	Roosevelt	P-meso	meso	0 0 0	101	—	0.24
4/30/78	Marlow	P-meso	meso	0 0 0	62	—	0.14
5/22/81	Granite	P-meso	T-meso	0 0 0	41	—	0.05
4/29/78	Castle	P-meso	T-meso	0 0 0	31	—	0.00
5/22/77	Bessie	P-meso	P-meso	0 0 0	28	—	0.00
4/29/78	Ada II	Couplet	Couplet	0 0 0	42	—	0.00

Tornado intensities: W = weak (F0–F1); S = strong (F2–F3); V = violent (F4); meso = mesocyclone; T-meso = transient mesocyclone; P-meso = provisional mesocyclone; Couplet = 3D couplet.
Maximum ERKE: Δt = 5 min, h = 0–7 km, S_m = 0.007 s^{-1}
? = Tornado damage survey incomplete. Tornado intensities are estimated.
* = Storm incompletely sampled.

There is a one-to-one correspondence in classification between algorithmic and manual analyses in 19 of the 26 total cases. Among the more rigorously defined mesocyclones (part A of Table 1), there is agreement in 17 out of 20 cases, and there is a one-to-one agreement among all the tornadic storms. Errors by the algorithm tend to be in the direction of underclassification. This is not surprising, since the algorithm technique for determining mesocyclone velocity couplet end points tends to underestimate mesocyclone peak velocities somewhat (appendix A). The discrepancies correspond to the weakest and least-developed features of the sample.

In general, mesocyclone formation precedes tornado development, and this is supported by our data. Lead times between mesocyclone classification by the algorithm and the first tornado of any intensity ranged from 2 min for Fort Cobb to 103 min for Binger, with a median of 36 min. However, if a forecast were based on mesocyclone identification alone, this would result in a false-alarm rate of 16/23 or 0.70.

The algorithm tracked a total of 2027 features. In the ascending hierarchy of feature organization discussed in section 5c, these comprised 252 shear features, 869 2D couplets, 705 3D couplets, 149 provisional mesocyclones, and 52 mesocyclones. Many of the storms had multiple mesocyclone cores as described by Burgess et al. (1982). Each of these were tracked separately. The average track duration for all features was 21 min. Mesocyclone tracks averaged 70 min. The longest tracks were shared by the Binger and Piedmont mesocyclones: 31 volume scans, corresponding to 3 h each.

Examples of the generated mesocyclone tracks are shown in Fig. 7 for Piedmont and Rush Springs, which occurred within one hour of each other. Thicker lines delineate locations where the feature was identified as a mesocyclone by the algorithm. Mesocyclone locations determined through visual inspection are within 0.8 km of the corresponding locations specified by the algorithm for these storms, and within 2.1 km for all storms. The location discrepancy is attributed to the

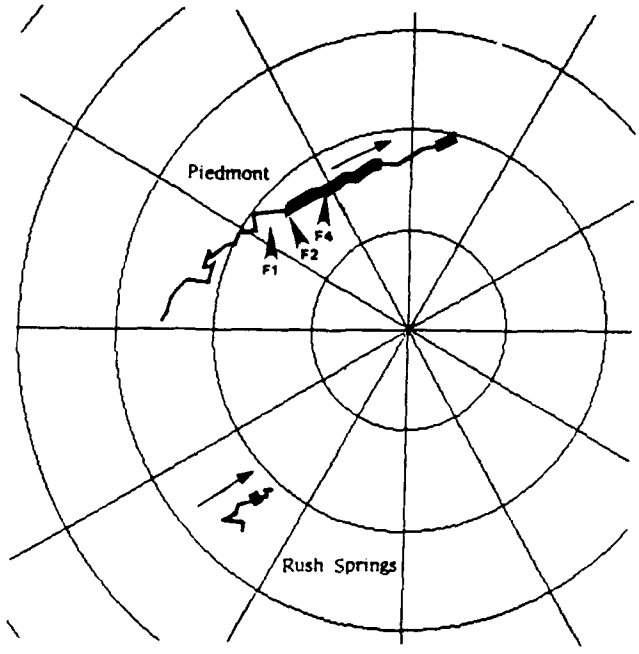

FIG. 7. Mesocyclone tracks as generated by the algorithm. Range circles are at 30-km intervals from the radar. Thicker lines indicate where the algorithm identified the feature as a mesocyclone. Arrows show general storm motion. Labeled arrowheads indicate tornado touchdown locations and F-scale intensities. Only the track associated with the most intense mesocyclone of each storm is shown.

3D feature construction process that forces a "best fit" when there is more than one possible combination; 2D features with the greatest ERKE are combined into one 3D feature. Tornado touchdown locations were, on average, within 3.8 km of the mesocyclone center.

Tracking is based on ERKE as discussed in appendix A. The quality of tracks prior to mesocyclone formation, when ERKE is very small, gives an indication of how well the technique works. Piedmont is a good example. A weak velocity couplet that preceded the mesocyclone for 90 min was tracked over 42 km by the algorithm.

b. Tornado prediction

Three-dimensional ERKE, shear, and velocity are examined as possible tornado predictors. Determination of the best performers was accomplished using two interpretation methods. The Student's t distribution, a statistical evaluator suitable to small samples, was used to determine the significance between means of maximum predictor values of mesocyclones with tornadoes and those without. This technique is explained in the appendix of our earlier paper (Donaldson and Desrochers 1990). Statistics help to narrow the contenders. A brute force approach is then adopted to select the best overall performer. We determine which integration heights, persistence times, and shear thresholds (for ERKE) provide the greatest lead times with fewest errors.

The vast majority of features the algorithm detects are inconsequential to tornado development, and simple criteria help to eliminate these. As an obvious starting point, all features that are identified by the algorithm as mesocyclones are evaluated for tornado potential. However, we do not feel it would be prudent to restrict the stage to mesocyclones. For one thing, mesocyclone classification is highly threshold dependent. Small measurement errors can adversely affect the classification process. Also, it is our experience that mesocyclone classification does not always provide as timely a warning for tornadoes as does an intensity evaluator like ERKE. In Piedmont, for example, ERKE achieved a significant magnitude before the mesocyclone could be verified.

In addition to mesocyclones, predictor values of 3D couplets and provisional mesocyclones are considered for tornado evaluation purposes. This criterion was used to test the algorithm, but in the interest of not overselling the results, we apply further restrictions here to evaluate the statistical performance of the algorithm. The performance evaluation is limited to storms with algorithm-identified mesocyclones (which number 20 in Table 1a, seven of them tornadic), and five other storms without mesocyclones (which include Roosevelt in Table 1b and four other unnamed ones) that have maximum ERKE or velocity greater than the mean of the nontornadic mesocyclones of the sample.

The three initial contending predictors are narrowed to two using the Student's t-test and a consideration of lead time and resolution errors. ERKE is our best statistical performer for the strong tornadoes, with a t value of 4.31 compared to 3.46 for velocity and 2.02 for shear. Values of t over 2.81 are significant at the 99% level for a sample size of 25 (23 degrees of freedom), and t values above 3.77 are significant at the 99.9% level. Velocity and especially ERKE are therefore both respectable performers. For the two violent tornadoes, shear produces the best t score: 4.35 compared to 3.68 for ERKE and 3.37 for velocity. These are determined using the maximum values occurring any time during the Piedmont and Binger storms. If we consider the maximum values *before* tornado touchdown, the t values drop to 3.53 for shear, 2.93 for velocity, and 3.52 for ERKE. This corresponds to a 19% reduction for shear, 13% for velocity, but only 4% for ERKE, and demonstrates that shear and velocity tend to achieve their most distinctive magnitudes while a violent tornado is on the ground. ERKE, on the other hand, achieves nearly as large values prior to tornado formation. We argue further against the use of shear for tornado prediction because it is the predictor most susceptible to error with degrading resolution, which is significant because on many occasions only a partial correction for resolution can be applied. As resolution decreases, size is overestimated and velocity underestimated. These work together to yield a larger error for shear. Velocity is somewhat less affected by resolution.

ERKE is affected the least of all since it is a function of the *product* of vortex velocity and size. In addition, ERKE is tailored for larger features, where sampling problems are less severe. With shear especially, maximum values occur with very small features that are unlikely to be positioned for optimum sampling.

Figures 8 to 10 show lead times for various tornado intensities versus errors comprised of misses (M) and false alarms (FA). The two kinds of errors are easily distinguished. The plots sloping upward to the right indicate errors due to false alarms, while those sloping downward indicate errors due to misses. While any tornado miss may be considered unacceptable, a tradeoff can be made between lead time and false alarms, as seen in the figures. These results assume that radar volumes were collected every 6 min and that the algorithm analysis was available simultaneous with the completion of each volume.

Figure 8 presents the median lead time to the first strong tornado of a storm. The median tornado lead time is presented rather than the mean in order to not overly bias the results by Binger, which provided a lead time that was at least double that of its nearest competitor over all error rates. ERKE, at a persistence time (Δt) of 5 min, an integration height (Δh) of 0–7 km, and a shear threshold (S_m) of 0.007 s^{-1}, provides a median lead time of 27 min with no errors. Velocity (Δt = 5 min, Δh = 0–7 km) and shear (Δt = 5 min, Δh = 0–7 km) achieve decent lead times, 19 and 29 min, but with an error rate of 0.12.

With ERKE at the threshold setting given above, Del City and Fort Cobb, the weakest of the tornadic storms, achieved negative lead times averaging −15 min in the error range of 0 to 0.08. We find that the use of a smaller shear threshold (S_m = 0.005 s^{-1}) and integration height (Δh = 0–4 km) provides much-improved lead times for the first tornadoes of these storms, although at the expense of a reduced median lead time for all the storms (10 min compared to 27 min). Figure 9 compares lead times versus errors for Del City and Fort Cobb for the standard ERKE thresholds and for the reduced thresholds. Increased lead times are produced by the reduced thresholds for all error rates. At error rates below 0.1 the *increase* in lead time averages 16 min. An average of 4 min lead time is provided for the first of the Del City and Fort Cobb tornadoes at an error rate of 0.1. These results suggest that the depth over which the mesocyclone intensifies prior to tornado formation may vary as a function of the resultant intensity of subsequent tornadoes.

Decent performance is achieved by all three predictors for the F4 Piedmont tornado. Errors in this case are due entirely to false alarms (Fig. 10). Piedmont is presented instead of Binger because its achieved performance is more conservative. ERKE (same thresholds as for strong tornadoes in Fig. 8) yields 31-min lead time with no errors. Binger, in comparison, yields over 60 min! Shear (same thresholds as in Fig. 8) and velocity (Δt = 10 min) are likewise respectable performers, producing no errors and lead times of 28 and 23 min. ERKE provides an average lead-time advan-

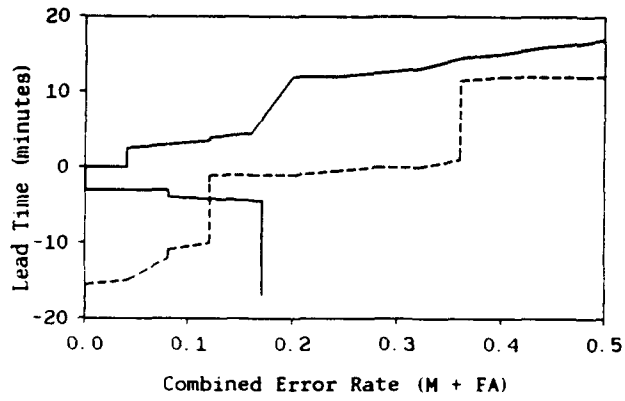

FIG. 9. Average lead time versus errors for the first tornado of Del City and Fort Cobb by ERKE. Solid lines are for Δh = 0–4 km and S_m = 0.005 s^{-1}. Dashed lines are for Δh = 0–7 km and S_m = 0.007 s^{-1}. Δt = 5 min for both.

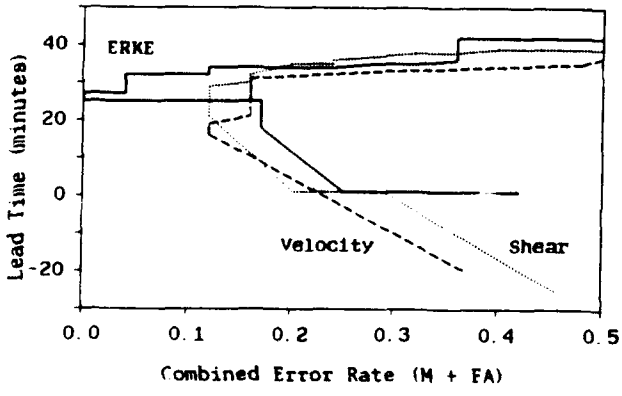

FIG. 8. Median lead time to the first strong tornado of a storm versus errors comprised of misses and false alarms (M + FA) provided by ERKE (solid lines), velocity (dashed lines), and shear (dotted lines). ERKE is calculated for Δt = 5 min, Δh = 0–7 km, S_m = 0.007 s^{-1}. Velocity represents Δt = 5 min and Δh = 0–7 km. Shear is determined for Δt = 5 min, Δh = 0–7 km.

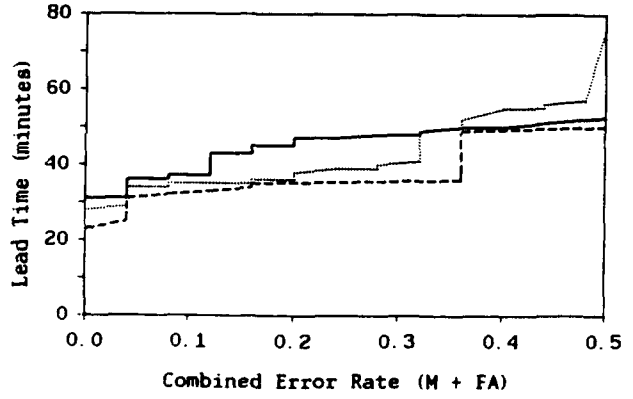

FIG. 10. Lead time versus errors for the Piedmont, Oklahoma, storm provided by ERKE, velocity, and shear (same notation and thresholds as in Fig. 8 except that Δt = 10 min for velocity).

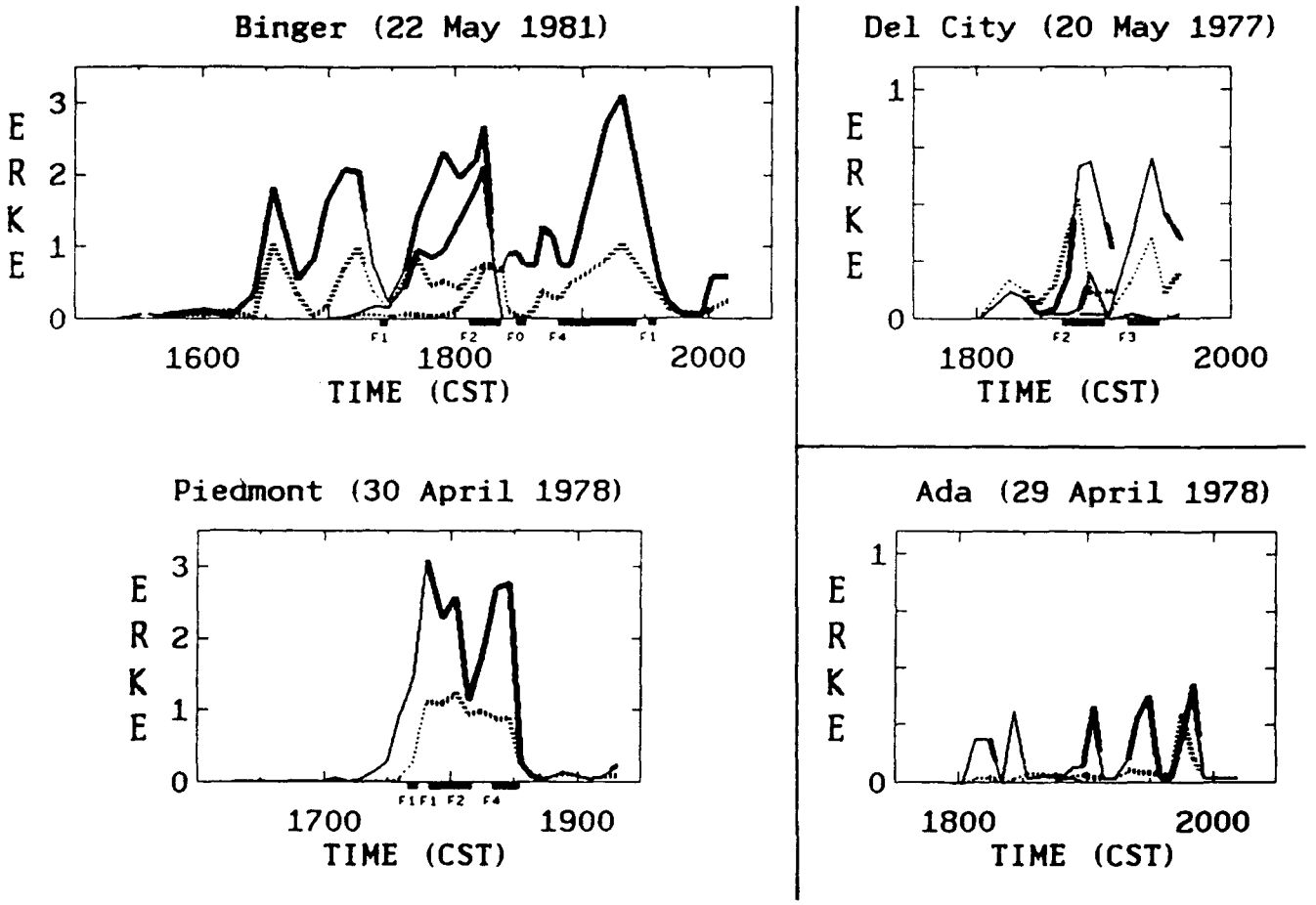

FIG. 11. ERKE growth curves for Δt = 5 min, Δh = 0–7 km, and S_m = 0.007 s^{-1} (solid lines), and Δt = 5 min, Δh = 0–4 km, and S_m = 0.005 s^{-1} (dotted lines). Examples are for violently tornadic storms (Binger and Piedmont), a strong tornado-producing storm (Del City), and a nontornadic storm (Ada).

tage of 5 min over shear and 9 min over velocity for error rates up to 0.3.

ERKE growth curves can help to further dichotomize the sample. Figure 11 presents examples of the evolution of our violently tornadic, strong tornado-producing, and nontornadic storms. Solid lines in the figures are for 5-min persistent values of ERKE at 0–7 km and 0.007 s^{-1}; dashed lines are for 0–4 km and 0.005 s^{-1}. (Recall that ERKE is normalized by units of CMM, the ERKE of a climatological mature mesocyclone. We are concerned here with 3D ERKE, and we normalize by the appropriate energy value: 1 CMM for 0–7 km and 0.007 s^{-1} = 6.1 × 10^{11} J; 1 CMM for 0–4 km and 0.005 s^{-1} = 2.1 × 10^{12} J.)

Binger and Piedmont display significant intensification at low levels, but the greatest intensification before tornado formation occurs in midlevels. In Del City, the greatest intensification eventually occurred in midlevels (0–7 km—note the change in ERKE scale compared to Piedmont and Binger), but the initial intensification at low levels provided increased lead times for the first tornado. In Ada, which is among the most intense of our nontornadic storms, moderate midlevel intensification was observed, but the mesocyclone never intensified significantly at low levels.

From Figs. 8–10 one can select an acceptable error rate to achieve a corresponding range of tornado lead

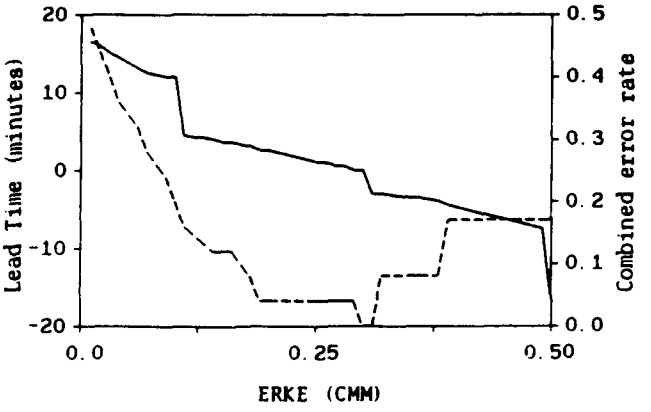

FIG. 12. Average performance by ERKE (Δt = 5 min, Δh = 0–4 km, and S_m = 0.005 s^{-1}) for the first tornadoes of the Del City and Fort Cobb mesocyclones. Solid lines show average lead times versus ERKE value. Dashed lines show errors corresponding to ERKE value.

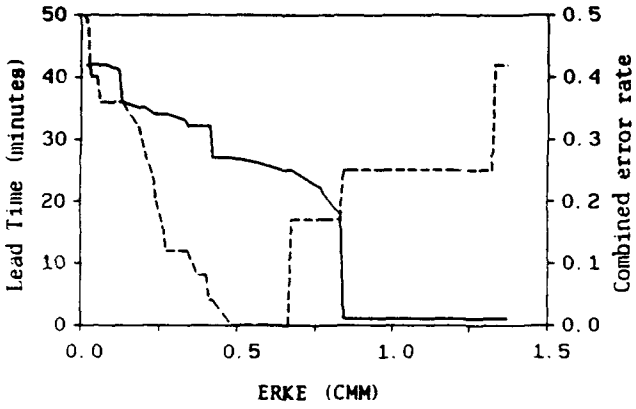

FIG. 13. Median performance for the first strong tornado of a storm by ERKE (Δt = 5 min, Δh = 0–7 km, and S_m = 0.007 s^{-1}). Solid lines show average lead times versus ERKE value. Dashed lines show errors corresponding to ERKE value.

times. An important aspect of performance is the sensitivity to a particular predictor value to deliver a given level of performance. For ERKE, the larger the range of CMM values for a certain level of performance is, the less sensitive the technique will be to spurious data or erroneous analysis. ERKE value sensitivity is presented in Figs. 12 and 13 for strong tornadoes, and in Fig. 14 for the violent tornadoes. Solid lines indicate lead times versus ERKE value in units of CMM. Dashed lines indicate the corresponding error rate.

Del City and Fort Cobb comprise the low quartile of performance. Average performance of these is given in Fig. 12 for Δt = 5 min, Δh = 0–4 km, and S_m = 0.005 s^{-1}. If no errors (misses and false alarms) are permitted, there is no lead time provided for these tornadoes. For error rates of 0.1 or less, average lead times up to 3 min are possible over an ERKE spread of 0.12 CMM. However, at an error rate of 0.3 or less, a maximum of 12-min lead time is provided. ERKE, therefore, shows some skill even for our worst performers, although the lead time is very short. In comparison, mesocyclone detection alone provides 17-min lead time for the low-quartile tornadoes, but at a false-alarm rate of 0.70.

Improved performance is achieved for the median lead time to the first strong tornado of the entire dataset. An error rate of 0.1 or less provides a median lead time of 28 min over an ERKE spread of 0.30 CMM (Fig. 13). As the ERKE spread increases, performance becomes less affected by measurement errors. As tornado intensity increases, the sensitivity to threshold selection decreases further. For F4 tornadoes (Fig. 14), a minimum lead time of 32 min with an error rate of 0.1 is achieved over an ERKE spread of 1.75 CMM!

7. Conclusions

An improved algorithm for automatic mesocyclone detection is presented that offers increased sensitivity and accuracy compared with earlier designs. This is achieved, in part, by minimizing the reliance on rigorous thresholds. Resolution-adjustable thresholds, used to filter pattern vectors, permit marginal mesocyclones of average size (5-km diameter) to be detected to a range of about 150 km. A weighting technique for mesocyclone core parameters provides estimates of rotational velocity that are generally within 4% of our visually derived estimates. Mesocyclone parameters are corrected for resolution where possible. Algorithm sensitivity automatically adjusts to the intensity of features observed.

The algorithm was tested on data containing 23 Oklahoma mesocyclonic storms that were verified by subjective analysis of the Doppler fields. The seven tornadic storms within this sample were detected with a median lead time of 36 min between incipient mesocyclone detection and the development of the first tornado. This result compares favorably with our determination by subjective analysis. However, tornado warning by mesocyclone identification alone provides an unacceptably high false-alarm rate, since 70% of the mesocyclonic storms were nontornadic. Mesocyclone classification overall was achieved with a false-alarm rate of 4% and a probability of detection of 83%. Classification errors were generally associated with very weak features, where small discrepancies in measurement can result in greatly different determinations of mesocyclone classification. With all detection failures a provisional mesocyclone was detected but the persistence to achieve mesocyclone classification was not realized.

The primary focus of this work has been the implementation of a tornado prediction algorithm. This is accomplished using a mesocyclone quantifier called ERKE, a variant of rotational kinetic energy tailored for the high shear of mesocyclones. ERKE provides the best capability to date for distinguishing between tornadic and nontornadic mesocyclones. Although our

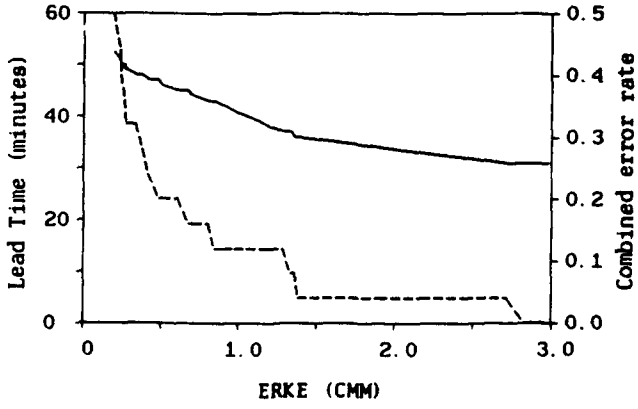

FIG. 14. Performance for the Piedmont F4 tornado by ERKE (Δt = 5 min, Δh = 0–7 km, and S_m = 0.007 s^{-1}). Solid lines show average lead times versus ERKE value. Dashed lines show errors corresponding to ERKE value.

sample is very small, our results appear to offer a decisive tornado warning tool. Low- to midtropospheric integrated ERKE, 0–7 km, persistent over a 5-min period, is distinctive and significant at the 99% level for violent tornadoes and at the 99.9% level for strong and violent tornadoes! For this limited sample of mesocyclonic storms, a median lead time of 27 min for strong tornadoes and a minimum of 31 min for violent tornadoes were achieved, with zero false alarms.

There is some indication that the height up to which low-level mesocyclone intensification extends may be further related to the intensity of the tornado produced. The best lead times for our lowest-quartile tornadic storms were achieved with ERKE integration over 0–4 km. This provided a 16-min improvement (4-min lead-time average for a false-alarm rate of 10%) for these storms over what was achieved with the 0–7-km ERKE integration. A much larger sample is needed to determine the generality of all of these findings. At any rate, the quantitative assessment of mesocyclone strength provided by the algorithm shows promise as a useful and effective technique for identifying tornado hazards associated with mesocyclonic storms. Such a tool as ERKE could be of particular assistance to a forecaster, especially in tornado outbreak situations like the ones examined here.

Acknowledgments. We are grateful to Dr. F. Ian Harris of Hughes STX Corporation and Mr. Kenneth M. Glover of Phillips Laboratory (PL) for their incitant suggestions. Their encouragement helped to make this work possible. Ms. Donna Velardi of PL assisted in the preparation of our manuscript. We have benefited from numerous discussions with Mr. Donald W. Burgess of the NEXRAD Operational Support Facility [formerly of the National Severe Storms Laboratory (NSSL)] during the development of this work. Don also provided some of our data. Useful comments were provided by reviewers Dr. Robert A. Maddox of NSSL and Dr. Louis W. Uccellini (co-editor of this journal). Their suggestions are much appreciated. This work was partly supported under PL Contract F19628-90-C-0088.

APPENDIX A

Technical Aspects of the Algorithm

1. Pattern vectors

The first step in mesocyclone detection is the identification of pattern vectors. We use thresholds of velocity difference (10 m s^{-1}) and shear (0.003 s^{-1}) measured between the pattern vector end points. The velocity difference threshold permits essentially the entire core region of a small and weak mesocyclone (defined by a 3-km diameter and a shear of 0.005 s^{-1}) to be detected. Azimuthal shear is constant in the core, but for such a mesocyclone the azimuthal velocity difference will vary from 15 m s^{-1} across the core center to as low as 10 m s^{-1} at other locations where solid-body rotation transitions to potential flow (Figs. 1b and 2). The detection of weak mesocyclones is important because, although these storms do not pose a particular tornado threat, many of them do produce other severe weather events.

The acceptable shear threshold for retention is fixed at less than mesocyclonic shear, in order to improve the detection of weak or developing mesocyclones and those that have components of divergence; the algorithm sometimes detects couplets associated with developing rotation half an hour or more before a mesocyclone is identified. This increased sensitivity comes at the cost of a 50% average increase in the number of detected pattern vectors and could be detrimental to algorithm performance if it resulted in a filling of the algorithm's capacity before all the existing vectors were detected. To prevent this, pattern vectors with shear less than mesocyclonic are considered expendable if the buffer should become full. However, in limited tests on extreme cases, we found the algorithm's capacity of 5000 pattern vectors per elevation to be generally sufficient.

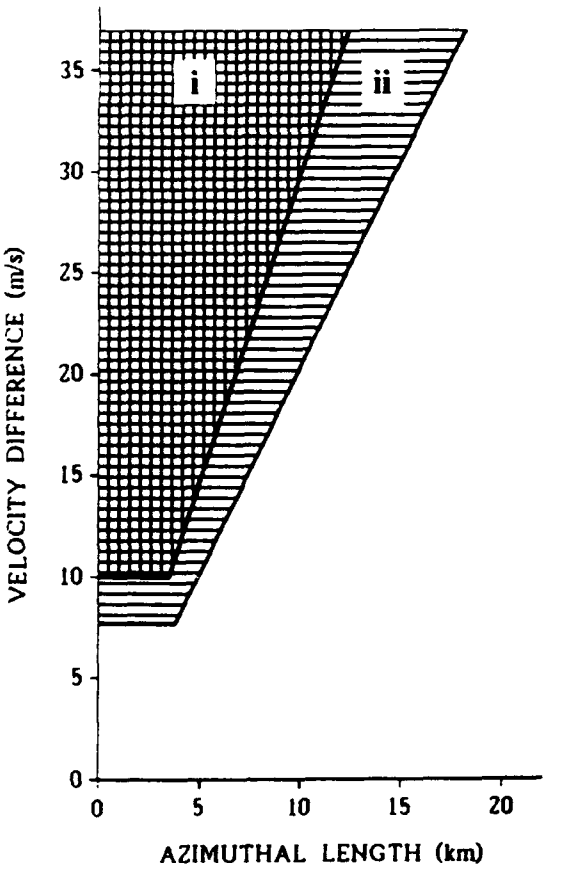

FIG. 15. Detection limits for pattern vectors. Region i indicates acceptable values of velocity difference and azimuthal diameter for pattern vector thresholds of 10 m s^{-1} and 0.003 s^{-1}. Region ii indicates the increased detection capability when resolution correction is applied for $BW/CR \leq 1$.

Pattern vector thresholds are adjusted for radar resolution according to Brown and Lemon's (1976) model of how a Rankine combined vortex would appear with varying resolution. Acceptable values of velocity difference and shear (in terms of pattern vector length) are presented in Fig. 15. Region i indicates the range of acceptable values if no correction for resolution were applied. Region ii indicates a further increase in detection capability when resolution correction is applied up to BW/CR = 1, assuming a pencil-beam radar with a half-power beamwidth of 1°.

2. Determination of two-dimensional feature characteristics

Pattern vectors that are close in radial proximity (≤1 km) and have azimuthal overlap are combined into a 2D feature. Feature parameters, such as size and rotational velocity, are then determined. For quantitative comparisons among storms, it is necessary that these estimations are accurate. Generally, very few of the pattern vectors that comprise a mesocyclone velocity couplet contain information of the maximum mesocyclone velocities. Therefore, a technique was developed to isolate the 2D couplet velocity maxima.

The sum of pattern vectors in a feature defines its pattern vector envelope and helps to distinguish feature type. In rotating features of mesocyclone size, only a few of the vectors contain the maximum relative incoming and outgoing velocities that are needed to describe the rotation. Since an analysis based on only a few points would be overly susceptible to spurious data, we consider a larger number of points, as is done in visual analysis through contouring of the velocity field. The technique developed is self-regulating in terms of the number of points included in the analysis. This number varies according to the size of the feature and the distribution of velocity values.

The velocity maxima of a couplet are determined from a selected sample of pattern vectors. Considering the relative incoming and outgoing regions of the couplet separately, a pattern vector is included in the sample if its magnitude is within some threshold velocity (V_{thresh}) of the maximum velocity of all the pattern vectors (V_{max}) of a feature. Each qualifying velocity (V_q) is then adjusted by the weighting function (W):

$$W = V_{\text{thresh}} - |V_q - V_{\text{max}}|, \tag{3}$$

where W is confined to $0 \leq W \leq V_{\text{thresh}}$. The velocity ($V$), azimuth (Az), and range (Rng) of each side of a velocity couplet are given by

$$V = \sum_{\text{all } V_q} (W)(V_q) / \sum_{\text{all } V_q} (W), \tag{4}$$

$$\text{Az} = \sum_{\text{all } V_q} (W)(\text{azimuth}) / \sum_{\text{all } V_q} (W), \quad \text{and} \tag{5}$$

$$\text{Rng} = \sum_{\text{all } V_q} (W)(\text{range}) / \sum_{\text{all } V_q} (W). \tag{6}$$

Values obtained in this way are weighted by the largest velocities. Nominally, V_{thresh} is 5 m s^{-1} and is increased by 5 m s^{-1} intervals until at least 10 points are identified, up to a maximum arbitrary threshold of 25 m s^{-1}. The lower threshold facilitates the detection of small and weak mesocyclones. The velocity couplet analysis technique underestimates rotational velocity by 4% on average for features that are well defined. Velocity is underestimated to a greater degree in features that are poorly defined. Therefore, there is an implicit bias toward well-developed mesocyclones.

Knowledge of the velocity couplet end points permits the mesocyclone diameter, orientation angle (θ), and rotational velocity to be determined (section 5a). Again, the Brown and Lemon (1976) model is used to normalize the mesocyclone parameters. Resolution adjustments are made for all features according to their beamwidth to core-radius ratio, with a maximum adjustment applied at BW/CR = 1 and the same adjustment applied for greater ratios. The Brown and Lemon model applies only to rotation. There is currently no comparable resolution-correction techniques for divergence. Therefore, the actual resolution correction applied is the total correction warranted by BW/CR multiplied by the cosine of θ. Features displaying pure rotation ($\theta = 0°$) receive the maximum correction, purely divergent features ($\theta = 90°$) receive no correction, and there is a smooth transition in between. It is felt that these approaches provide conservative corrections for resolution and avoid overcompensating for poor resolution.

3. Hierarchy of features

Algorithm sensitivity, through pattern vector thresholds, is such that numerous features are detected, many of which are insignificant. A limited algorithm capacity for features necessitates a hierarchy to assure that significant features are retained. ERKE is an effective element in such a hierarchy. Generally, ERKE associated with shear features and couplets is strikingly small compared with mesocyclones. Feature shape is another distinguishing quality of mesocyclones. The pattern vector envelope of mesocyclones tends to be relatively equal in azimuthal and radial dimensions. Where ERKE is very small or zero, as it would be for premesocyclonic rotation, feature shape is determinant of a favored position in feature hierarchy. Therefore, each feature is categorized according to the following hierarchy parameter:

For 2D ERKE > 0, Hierarchy value

$$= (\text{Shape})(\text{ERKE}); \tag{7}$$

for 2D ERKE = 0, Hierarchy value = Shape. (8)

Shape is a function of the maximum azimuthal and radial dimensions of the pattern vector envelope. The ratio is the shorter dimension over the longer. Shape is therefore constrained between 0 and 1.

ERKE in (7) is for a shear threshold of 0.005 s^{-1} and is normalized by units of CMM. It is felt appropriate to give more weight to feature energy than to shape and, therefore, ERKE in (7) has units of CMM multiplied by 100. This ERKE weighting factor is arbitrary but not critical. It was found to be effective for features observed during testing.

4. Tracking

Persistence criteria for mesocyclone detection and for tornado prediction are satisfied with a simple tracking routine. Features from consecutive volume scans are associated into what we term a *time-series feature*. Association is based on proximity and ERKE. A proximity condition is necessary for tracking, but used alone it proves unsatisfactory because of the abundance of velocity features within storms. ERKE distinguishes the significant features.

Only two consecutive volume scans are required for tracking, but each feature may be tracked, if necessary, for up to 40 volume scans. Features from consecutive volumes may be associated if their centers are separated by a threshold distance of $\leq$15 km. Preference is given to higher-energy features. The reference 3D ERKE used for tracking is arbitrary and is that calculated from 0 to 7 km at a shear threshold of 0.005 s^{-1}.

It is common for a storm to contain multiple mesocyclone cores (Burgess et al. 1982), and the algorithm tracks each core as a separate entity. However, the most intense mesocyclone cores of a storm will generally be associated within the same track. This occurs because the distance threshold for tracking can span the distance between the older and newer updrafts for moderately moving storms. Tracking in this way is not believed to be detrimental. The work of Donaldson and Desrochers (1990) suggests that tornado intensity corresponds to the maximum mesocyclone energy in a storm. The threshold is suitable to NEXRAD, where update times of 5 min are available. The threshold also allows for a feature placement error of a few kilometers.

APPENDIX B

Preprocessing

For this study, velocity data were filtered of noise and corrected for aliasing prior to processing by the present algorithm. This was accomplished with a two-dimensional technique by Desrochers (1990). This dealiasing algorithm is quite suited to the problem at hand as it is particularly accurate for mesocyclones; 98% of mesocyclone scans are found to be correctly processed.

Some of the data were contaminated by radar-beam sidelobes. This was especially a problem with Ada (29 April 1978), which was not tornadic but produced 10-cm hailstones. The sidelobes, which were associated with a high-reflectivity core in excess of 60 dBZ, contaminated the velocity field on multiple elevations. The result was a spurious signal that was mistaken as a mesocyclone by the algorithm. Thresholding of the velocity data at 15 dB above noise was found to successfully eliminate the spurious feature and still permit detection of the Ada mesocyclone. Sidelobes are a radar problem that need to be addressed in preprocessing. Improved sidelobe characteristics, expected with NEXRAD, may alleviate this kind of problem. At any rate, sidelobes can affect algorithm performance because at the level of processing that the algorithm operates it is not possible to distinguish spurious data persisting for two or more consecutive volume scans.

It would be preferable if it were not required to apply a received power threshold to the velocity data. This is because mesocyclones often contain weak echo regions (WER) (e.g., Browning 1965), where the reflectivity may be very close to the noise level. For the most part, however, an echo-weak area comprises only a small part of a mesocyclone, and the mesocyclone circulation may still be detected if the velocity data associated with it is ignored. Of course, incomplete sampling of the mesocyclone can result in poor estimation of core size and rotational velocity.

There was also the problem of ground clutter near the radar. Data were ignored within 15 km of the radar and for the first 15 km beyond the first velocity trip. It is expected that the clutter-suppression techniques developed for NEXRAD will greatly reduce if not eliminate this problem.

REFERENCES

Atlas, D., 1963: Radar analysis of severe storms. *Meteor. Monogr.*, **5**, 177–220.

Bluestein, H. B., 1985: The formation of a "landspout" in a "broken-line" squall line in Oklahoma. Preprints, *14th Conf. on Severe Local Storms*, Indianapolis, Amer. Meteor. Soc., 267–270.

Brady, R. H., and E. J. Szoke, 1989: A case study of nonmesocyclone tornado development in northeast Colorado: Similarities to waterspout formation. *Mon. Wea. Rev.*, **117**, 843–856.

Brandes, E. A., 1978: Mesocyclone evolution and tornadogenesis: Some observations. *Mon. Wea. Rev.*, **106**, 995–1011.

——, 1981: Finestructure of the Del City–Edmond tornadic mesocirculation. *Mon. Wea. Rev.*, **109**, 635–647.

Brown, R. A., and L. R. Lemon, 1976: Single Doppler radar vortex recognition: Part II—Tornadic vortex signatures. Preprints, *17th Conf. on Radar Meteorology*, Seattle, Amer. Meteor. Soc., 104–109.

——, and V. T. Wood, 1991: On the interpretation of single-Doppler velocity patterns within severe thunderstorms. *Wea. Forecasting*, **6**, 32–48.

——, L. R. Lemon, and D. W. Burgess, 1978: Tornado detection by pulsed Doppler radar. *Mon. Wea. Rev.*, **106**, 29–38.

Browning, K. A., 1965: Some inferences about the updraft within a severe local storm. *J. Atmos. Sci.*, **22**, 669–677.

Burgess, D. W., 1976: Single Doppler radar vortex recognition: Part I: Mesocyclone signatures. Preprints, *17th Conf. on Radar Meteorology*, Seattle, Amer. Meteor. Soc., 97–103.

——, and R. J. Donaldson, Jr., 1979: Contrasting tornadic storm types. Preprints, *11th Conf. on Severe Local Storms*, Kansas City, Amer. Meteor. Soc., 189–192.

——, and L. R. Lemon, 1990: Severe thunderstorm detection by radar. *Radar in Meteorology*, D. Atlas, Ed., Amer. Meteor. Soc., 619–647.

——, and ——, 1991: Characteristics of mesocyclones detected during a NEXRAD test. Preprints, *25th Conf. on Radar Meteorology*, Paris, Amer. Meteor. Soc., 39–42.

——, V. T. Wood, and R. A. Brown, 1982: Mesocyclone evolution statistics. Preprints, *12th Conf. on Severe Local Storms*, San Antonio, Amer. Meteor. Soc., 422–424.

Davies-Jones, R., 1984: Streamwise vorticity: The origin of updraft rotation in supercell storms. *J. Atmos. Sci.*, **41**, 2991–3006.

Desrochers, P. R., 1990: A technique for automated velocity dealiasing. GL-TR-90-0079, ADB150718, Phillips Laboratory, Air Force Systems Command, 109 pp.

——, 1991: Automated mesocyclone detection and tornado forecasting. PL-TR-91-2051, ADB156102L, Phillips Laboratory, Air Force Systems Command, 168 pp.

——, R. J. Donaldson, Jr., and D. W. Burgess, 1986: Mesocyclone rotational kinetic energy as a descriminator for tornadic and non-tornadic types. Preprints, *23rd Conf. on Radar Meteorology*, Snowmass, CO, Amer. Meteor. Soc., 1–4.

Donaldson, R. J., Jr., 1970: Vortex signature recognition by a Doppler radar. *J. Appl. Meteor.*, **9**, 661–670.

——, and P. R. Desrochers, 1985: Doppler radar estimates of the rotational kinetic energy of mesocyclones. Preprints, *14th Conf. on Severe Local Storms*, Indianapolis, Amer. Meteor. Soc., 52–55.

——, and ——, 1990: Improvement of tornado warnings by Doppler radar measurement of mesocyclone rotational kinetic energy. *Wea. Forecasting*, **5**, 247–258.

——, G. M. Armstrong, A. C. Chmela, and M. J. Kraus, 1969: Doppler radar investigation of air flow and shear within severe thunderstorms. Preprints, *6th Conf. on Severe Local Storms*, Chicago, Amer. Meteor. Soc., 146–154.

Fujita, T. T., 1981: Tornadoes and downbursts in the context of generalized planetary scales. *J. Atmos. Sci.*, **38**, 1511–1534.

Hennington, L. D., and D. W. Burgess, 1981: Automatic recognition of mesocyclones from single Doppler radar data. Preprints, *20th Conf. on Radar Meteorology*, Boston, Amer. Meteor. Soc., 704–706.

Holton, J. R., 1979: *An Introduction to Dynamic Meteorology*. Academic Press, 391 pp.

JDOP Staff, 1979: Final report on the Joint Doppler Operational Project (JDOP) 1976–1978. NOAA Tech. Memo., ERL NSSL-86, 84 pp.

Johnson, K. W., P. S. Ray, B. C. Johnson, and R. P. Davies-Jones, 1987: Observations related to the rotational dynamics of the 20 May 1977 tornadic storms. *Mon. Wea. Rev.*, **115**, 2463–2478.

Klemp, J. B., and R. Rotunno, 1983: A study of the tornadic region within a supercell thunderstorm. *J. Atmos. Sci.*, **40**, 359–377.

Lemon, L. R., and C. A. Doswell III, 1979: Severe thunderstorm evolution and mesocyclone structure as related to tornadogenesis. *Mon. Wea. Rev.*, **107**, 1184–1197.

——, and D. W. Burgess, 1980: Magnitude and implications of high speed outflow at severe storm summits. Preprints, *19th Conf. on Radar Meteorology*, Miami Beach, Amer. Meteor. Soc., 364–368.

Lhermitte, R. M., 1964: Doppler radars as severe storm sensors. *Bull. Amer. Meteor. Soc.*, **45**, 587–596.

NEXRAD Joint System Program Office (JSPO), 1986: NEXRAD Technical Requirements. JSPO Rep. No. R400-SP301, January.

NOAA, 1977, 1978, 1981: *Storm Data*. Vols. 19, 20, and 23, Environmental Data Services, NOAA, Asheville.

Ray, P. S., B. C. Johnson, K. W. Johnson, J. S. Bradberry, J. J. Stephens, K. K. Wagner, R. B. Wilhelmson, and J. B. Klemp, 1981: The morphology of several tornadic storms on 20 May 1977. *J. Atmos. Sci.*, **38**, 1643–1663.

Rotunno, R., 1981: On the evolution of thunderstorm rotation. *Mon. Wea. Rev.*, **109**, 577–586.

——, and J. Klemp, 1985: On the rotation and propagation of simulated supercell thunderstorms. *J. Atmos. Sci.*, **42**, 271–292.

U.S. Standard Atmosphere Supplement, 1966: U.S. Government Printing Office, Washington, D.C., ESSA, NASA, USAF, 289 pp.

Wakimoto, R. M., and J. W. Wilson, 1989: Non-supercell tornadoes. *Mon. Wea. Rev.*, **117**, 1113–1140.

Weisman, M. L., and J. B. Klemp, 1982: The dependence of numerically simulated convective storms on vertical wind shear and buoyancy. *Mon. Wea. Rev.*, **110**, 504–520.

Wieler, J. G., 1986: Real-time automated detection of mesocyclones and tornado vortex signatures. *J. Atmos. Oceanic Technol.*, **3**, 98–113.

Wilson, J. W., 1986: Tornadogenesis by non-precipitation induced wind shear lines. *Mon. Wea. Rev.*, **114**, 270–284.

Wood, V. T., and R. A. Brown, 1983: Single Doppler velocity signatures: An atlas of patterns in clear air/widespread precipitation and convective storms. NOAA Tech. Memo. ERL NSSL-95, 71 pp.

Zrnić, D. S., D. W. Burgess, and L. D. Hennington, 1985a: Automatic detection of mesocyclonic shear with Doppler radar. *J. Atmos. Oceanic Technol.*, **2**, 425–438.

——, ——, and ——, 1985b: Doppler spectra and estimated windspeed of a violent tornado. *J. Climate Appl. Meteorol.*, **24**, 1068–1081.